Soft Matter

Thermal Molecular Focusing: Tunable Cross effect of Phoresis and Light-driven Hydrodynamic Focusing

Journal:	*Soft Matter*
Manuscript ID	SM-ART-04-2018-000754.R1
Article Type:	Paper
Date Submitted by the Author:	05-Jun-2018
Complete List of Authors:	Fukuyama, Tatsuya; Kyushu University, Department of Physics Nakama, Sho; Kyushu University, Department of Physics Maeda, Yusuke; Kyushu University, Department of Physics

SCHOLARONE™
Manuscripts

Thermal Molecular Focusing: Tunable Cross effect of Phoresis and Light-driven Hydrodynamic Focusing

Tatsuya Fukuyama[1], Sho Nakama[1], and Yusuke T. Maeda[1,*]

[1]*Kyushu University, Department of Physics, Motooka 744, Fukuoka 819-0395, Japan*

(Dated: June 4, 2018)

The control of solute fluxes by either microscopic phoresis or hydrodynamic advection is a fundamental way to transport molecules, which are ubiquitously present in nature and technology. We study the transport of large solute such as DNA driven by a time-dependent thermal field in a polymer solution. Heat propagation of a heat spot moving back and forth gives rise to the molecular focusing of DNA with frequency-tunable control. We develop a model where viscoelastic expansion of a solution and viscosity gradient of a smaller solute are coupled, and that explains the underlying hydrodynamic focusing. This effect offers novel non-invasive manipulation of soft and biological materials in a frequency tunable manner.

INTRODUCTION

In 1951, the seminal work by G.I. Taylor has shown that the pumping in a viscous fluid can be driven by an undulating infinite sheet at a low Reynolds number, proposing that the flexible object can put into motion of a viscous fluid with a finite surface disturbance[1]. To date, a variety of analytical and numerical models for pumping in a viscous fluid have been developed [2], and the pumped flow of complex fluids has gained considerable attention from a fundamental perspective. A peristaltic flow through periodic contact compression using electromechanical[3] or opto-mechanical stresses[4] has been shown to be microfluidic modulators. In particular, a hydrodynamic force offers a versatile method for rapid mixing[5], particle trapping, and assembly[6] in a confined geometry with dimensions of tens or hundreds of micrometers, which has revolutionized fluid mechanics and soft-matter physics at the small scale as the core of nano- to microfluidic devices[7].

Although exploration beyond conventional methods is challenging, it is necessary for the development of new applications based on hydrodynamic forces. On the one hand, light-driven advection of particles has been demonstrated by using an infrared laser focusing. When a hot spot in a focused laser moves at a constant speed in a highly viscous solution, a net fluid flow occurs, owing to the coupling of thermally reduced viscosity and fluid compressibility[8][9][10][11]. Although this effect can convey particles, to be extended for the trapping of molecules, one requires a well-designed stagnation point under complex streamlines. On the other hand, microscopic phoretic transports such as thermophoresis[12][13][14][15] or diffusiophoresis[16][17][18][19][20][21][22], which is the transport along a gradient of temperature or concentration of a smaller solute respectively, is expected to be a versatile mean of molecular manipulation. Thermophoresis depletes a high concentration of a solute from a hot region and builds its concentration gradient. In such a solution, another solute of larger size experience both thermophoresis and diffusiophoresis as a secondary effect.

The balance of two phoretic motions allows one to control the direction and magnitude of the transport velocity to trap molecules[23][24][25]. Indeed, diffusiophoretic manipulation has the unique advantage of exhibiting low dependence on electromagnetic properties, because the driving force arises from the slip velocity on the particle surface[26][27]. However, the balance between counteracting transports has to be suitably adjusted by changing the temperature difference or solute concentration under the initial conditions, which could be a fundamental limitation. Conventional methods thus have exhibited particular advantages and limitations. Hence, further advances in our understanding regarding the interplay among phoretic transports and hydrodynamics are needed.

Here we report thermal molecular focusing where the cross-effect of phoretic transports and advective flow by a time-dependent thermal field realizes tunable molecular manipulation. The coupling of viscoelastic expansion of fluids due to boundary deformation and thermophoretic reduction of viscosity pumps the microflow in a polymer solution. Strikingly, novel hydrodynamic focusing is involved in frequency-tunable molecular focusing, without the need to adjust external parameters such as temperature and solute concentration.

EXPERIMENTAL SETUP

A. Optical setup

We built the following optical setup. Temperature gradient was built by focusing infrared laser (FOL1435R50-317, Furukawa Electronics, 1480 nm wavelength). Photons of 1480 nm wavelength are efficiently absorbed in water. The laser was focused using a 20× objective lens with long working-distance (NIKON) and deflected by a set of two galvo mirrors (Cambridge technologies). Other optical setups were purchased from Thorlabs. The chamber was viewed with an epifluorescence microscope (Olympus, IX73) with the stable excitation light source (Lumen Dynamics, XLED1). The tempera-
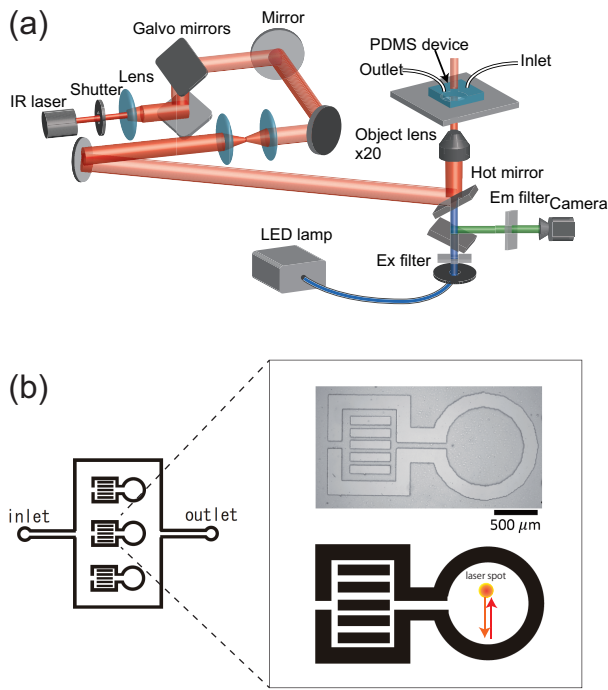
FIG. 1. Schematic illustration of (a) optical setup and (b) microfluidic device used in this study

ture of the microscope stage was kept at $T_0 = 24\pm0.1\,°C$. The temperature difference *in situ* $\Delta T(x,y) = T(x,y) - T_0$ was measured by calibrating the reduced fluorescent intensity of temperature-dependent fluorescein (2'-7'-bis(carboxyethyl)-5(6)-carboxyfluorescein, BCECF, Molecular probes) at the static temperature gradient. For this calibration we measured the fluorescent intensity of fluorescein at various temperatures from T=20 to $50\,°C$ by fluorescent spectrometer with a temperature control unit and then draw the curve for temperature calibration. The fluorescent intensity was decreased at the rate of -1.8%/K. We set the maximal value ΔT=9.6 K and gradient ∇T=0.08 K/μm. The laser spot was steered by using galvo mirrors back and forth along a line of $-L \leq x \leq L$ at a speed of u_l[26](FIG. 1(a)).

B. Microfabrication

The solution was entrapped in a chamber of 25 μm thickness and 800 μm in diameter made by standard soft lithography techniques described below. This small thickness suppresses the onset of thermal convection during laser irradiation and we have checked the effect from convective flow is negligible in a static temperature gradient as seen in previous studies[24][25][26][27]. The microfluidic devices made of silicone elastomer (Polydimethyl siloxane, PDMS, Sylgard 184, Dow Corning) with a PDMS-coated glass slide were filled with the polymer solution (FIG.1(b)). SU-8 photoresist was patterned with conventional UV photolithography method. The

patterned surface of SU-8 was transferred to PDMS chip by casting uncured PDMS mixed with curing agent and then cured for 1 hour at $75\,°C$. After the cutting PDMS chip with a scalpel, the chips were strongly bonded on the PDMS-coated glass slide by having their surfaces hydrophilic by plasma-gun surface treatment for 30 sec and then cured PDMS again by heating at $90\,°C$ for 1 hour. The inlet and outlet of PDMS device were connected with thin PEEK tubes from the pressure-regulated microfluidic pump (MFCS flow system, Fluigent).

C. Chemical reagents

We used DNA of 4.3 kbp as a large solute (gyration radius $a \approx 0.1\,μm$) with a concentration of $0.01\,wt\%$. The plasmid DNA was purified from *E.coli* bacteria by using conventional method. The polymer as a smaller solute dissolved in an aqueous solution is polyethylene glycol 20000 (PEG, its gyration radius $R_g^p \approx 2.5\,nm$, Alfa Aesar) at $5.0\,wt\%$ in Tris-HCl and 50 mM EDTA buffer solution (pH 7.2). The purified DNA was dissolved in the PEG solution and then stained by SYBR Gold dye (S11494, Molecular Probe) in order to quantitatively measure its local concentration. In order to avoid both evaporation of solvent content and bubble formation, the PEG solution was kept flowing continuously outside of the area for observation in the PDMS device.

D. Image analysis

Particle image velocimetry (PIV) is performed for the visualization of flow field. The tracer particle for PIV was the silica beads with 3.0 μm in diameter (Micromod, sicastar) and its mass fraction was set at $0.1\,wt\%$ in $5.0\,wt\%$ PEG solution. Time-lapse movie was taken by the interval of 3 sec and the obtained velocity field was analyzed by using ImageJ. In addition, fluorescent recovery after photobleaching (FRAP) was performed in order to determine the diffusion coefficient of DNA D in a PEG solution. Plasmid DNA in a PEG solution was enclosed within a chamber with a thickness of 30 μm. The DNA was visualized by a fluorescent nucleic acid stain (SYTOX-Orange, Molecular probes) and its concentration was measured by the fluorescent microscopy. A focused laser with a wavelength of 532 nm (25 mW, Cobalt laser) depleted the signal of the stained DNA around the focal point with a radius of 33.4 μm. Typical diffusion coefficients were 5.32 ± 0.31 μm^2/s in water, 2.67 ± 0.57 μm^2/s in $2.0\,wt\%$ PEG, and 1.06 ± 0.73 μm^2/s in $5.0\,wt\%$ PEG.

RESULTS AND DISCUSSION

E.   Focusing of DNA in a moving heat spot

We first present the basic phoretic transports in gradients of temperature and solute concentration, at a fast moving hot spot ($u_l \sim 10\,\mathrm{mm\,s^{-1}}$) along the linear path (FIG. 2(a)). The temperature gradient creates a concentration gradient of the smaller solute A at a large volume fraction (i.e., PEG in the present study). In such a solution, another large solute B of a very small volume fraction (i.e., DNA) is displaced away from the hot region. Given that solute B exhibits a steric repulsive interaction with solute A, diffusiophoretic transport caused by the concentration gradient of solute A tends to bring solute B back to the hot region, which results in the trapping of solute B[23][24][26]. Consistent with this mechanism, a temperature gradient made by a laser sweep creates a PEG concentration gradient, which, in turn, uniformly accumulates the DNA along the scanning path of $-L \leq x \leq L$ with $2L$=209 µm (FIG. 2(b))[24][26]. The DNA is also uniformly trapped along the path of the laser scanning even at a slower speed $u_l \sim 1\,\mathrm{\mu m\,s^{-1}}$. Because the speed of DNA diffusive escape is $D/w \approx 0.1\,\mathrm{\mu m/s}$ (the radius of the heated region $w \approx 50\,\mathrm{\mu m}$ and diffusion coefficient of DNA in the hot spot D=2.89 µm²/s), the laser sweeping with $u_l \geq 0.1\,\mathrm{\mu m\,s^{-1}}$ effectively accumulates the DNA. Although the trappings at two extreme cases are consistent with conventional phoretic transports, a new behavior was observed at the intermediate velocity ($u_l \sim 10^2\,\mathrm{\mu m\,s^{-1}}$). The DNA was accumulated not along the path of the moving hot spot, but at its mid-point, and was finally focused (FIG. 2(b) and (c)). The amount of focused DNA was controlled in a velocity-dependent manner, implying frequency-dependent modulation of molecular focusing. This finding motivated us to explore two questions: First, what effect can give rise to molecular transport based on the speed of a moving hot spot? Second, what is the underlying mechanism behind the focusing of DNA through a dynamic thermal gradient?

F.   Light-driven hydrodynamic focusing

It has been shown that net fluid flow occurs when a heat source moves in highly viscous solution[9][10][11]. A moving heat source propagates in one direction with periodic boundary conditions. When a localized hot spot moves at the speed u_l in a highly viscous solution (e.g., $80wt\%$ glycerol) confined within thin solid substrates (a height of a few microns), thermal expansion of the viscous fluid induces extensile and contractile flows at the front and rear edges of the hot spot, respectively. Although the isotropic viscosity prohibits the onset of net flow, thermally reduced viscosity in fluids enlarges the extensile flow at the front edge and the contractile flow at the rear edge. This imbalance eventually creates a
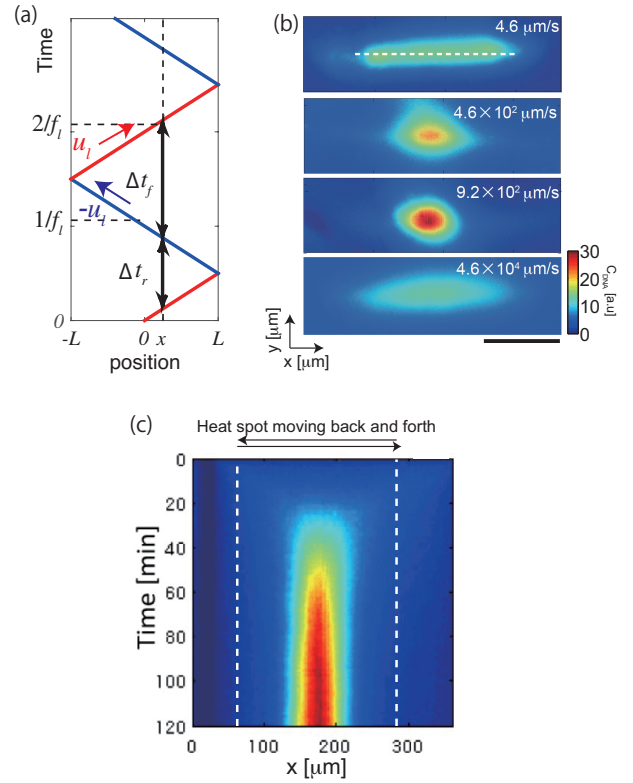

FIG. 2. Experimental demonstration of tunable molecular focusing of DNA using a moving hot spot in a polymer solution. (a) A single heat source moves in back and forth direction. It turns the direction of motion in the opposite direction at the edges $x = \pm L$. (b) DNA trapped by the temperature gradient moving back and forth at various speed u_l=4.6, 4.6×10^2, 9.2×10^2, and $4.6 \times 10^4\,\mathrm{\mu m\,s^{-1}}$ (from top to bottom). The white dashed line is the path of a moving laser spot. Scale bar: 100 µm. (c) Kymograph of molecular focusing of DNA at u_l=$9.2 \times 10^2\,\mathrm{\mu m\,s^{-1}}$. The white dashed lines are the edges of the path of a moving laser spot

net flow u opposite to the motion of the hot spot. The velocity of net flow is given by $u = \frac{u_l}{2}\alpha\beta(\Delta T)^2$ where $\alpha = \frac{1}{\rho}(\frac{\partial \rho}{\partial T})$ is thermal expansion coefficient of viscous fluid of density ρ and $\beta = \frac{1}{\eta}(\frac{\partial \eta}{\partial T})$ is thermal reduction of viscosity η[9]. This thermo-hydrodynamic flow at microscale (microflow) could be relevant to the observed thermal molecular focusing. However, this type of advection becomes zero after canceling each other out when the hot spot moves back and forth. To address the underlying mechanism in thermal molecular focusing, our key idea is to combine distinct disciplines, those are hydrodynamics, viscoelastic mechanics, and heat conduction, as formulated below.

Herein, we develop a model that leads to both molecular focusing and its tunable control in a moving heat source[28](FIG. 3(a)). A semi-dilute polymer solution is enclosed in a thin chamber with a deformable PDMS wall. Its viscosity, elastic modulus, and characteristic relaxation time are η^w, E, and $\tau = \eta^w/E$, respectively.
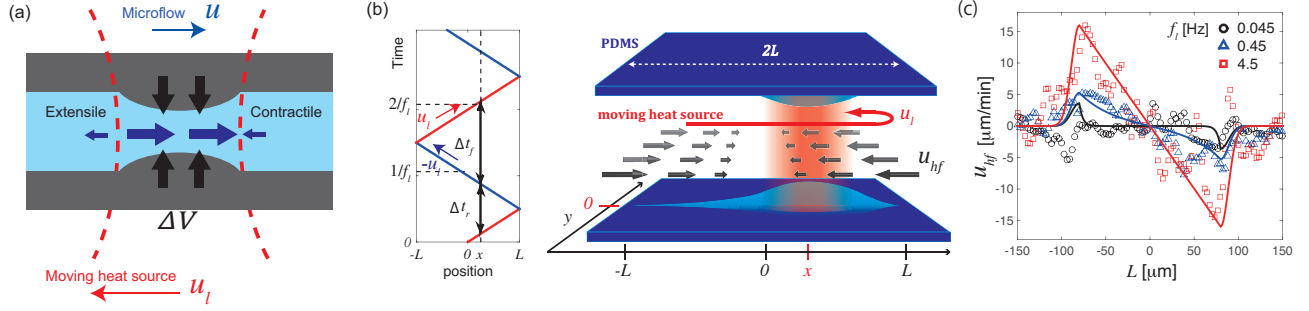
FIG. 3. Light-driven hydrodynamic focusing in a hot spot moving back and forth. (a) Schematic illustration of the microflow driven by thermal expansion of boundary wall and the squeezed polymer solution. (b) Schematic image of LHF through the coupling of thermal viscosity reduction and thermal viscoelastic expansion in a hot spot that moves in back and forth. (c) The profiles of LHF at f_l=4.5 × 10^{-2} Hz(black), 4.5 × 10^{-1} Hz(blue), 4.5 Hz (red). The solid lines are numerical calculations of Eq.(2) with $\tau = 1.2$ s [31].

The viscosity η of a polymer solution depends on the temperature and solute concentration. Once a temperature gradient is created in such a solution, the solute builds a local concentration gradient close to the heat source. It means that thermophoresis reduces the viscosity mediated by the local depletion of the solute. The rate of viscosity change as function of temperature, β, is defined as $\beta = \frac{1}{\eta}(\frac{\partial \eta}{\partial T} + \frac{\partial \eta}{\partial c}\frac{\partial c}{\partial T})$, where the first term represents the direct effect of the temperature rise and the second term describes the indirect effect due to thermphoresis. For a PEG solution, thermophoretic depletion allows one to have a more explicit form of β. In a temperature gradient of ∇T, the density flux J^p of a PEG solute is given by $J^p = -D^p(\nabla c^p + c^p S_T^p \nabla T)$ where c^p is the PEG concentration, D^p is the diffusion coefficient of PEG, and S_T^p is the Soret coefficient of PEG defined as D_T^p/D^p with the thermal diffusion coefficient of PEG of D_T^p[29](D^p=58 µm s^{-2} and S_T^p=8.89 × 10^{-2} K^{-1} in this study). It is known that the viscosity logarithmically increases with c^p[30]. One thus yields $\beta = \beta_0 + \beta_1 c_0^p S_T^p$ because $c^p = c_0^p \exp[-S_T^p \Delta T]$ where c_0^p is PEG concentration at infinity.

In addition, the walls in top and bottom deform upon the transferred heat at time $t = 0$, and thereafter the enclosed fluid is compressed. The strain relaxation of the deformed wall after Δt is set using $\epsilon_\tau(\Delta T, \Delta t) = \Delta V_\tau/V_0 \approx \gamma(1 - e^{-\Delta t/\tau})\Delta T$ where $\gamma = \frac{1}{V_0}\frac{dV}{dT}$ is the coefficient of thermal viscoelastic compression of solution squeezed by the expanded wall. By averaging over one period of thermal stimulation $1/f_l$, the microflow is given by

$$\boldsymbol{u} = -\boldsymbol{u_l}\frac{(\beta_0 + \beta_1 c_0^p S_T^p)\Gamma_\tau}{2}(\Delta T)^2. \quad (1)$$

where $\Gamma_\tau = \gamma(1 - e^{-1/f_l\tau})$ is thermal *viscoelastic* expansion coefficient of the solution with $\tau = 1.2$ sec[28][31]. We note that both β and Γ_τ have negative sign in present study.

We next consider the microflow in a sweeping laser spot back and forth (FIG. 3(b)). A heat source moves back and forth along a line ($-L \leq x \leq L$, $y = 0$,

2L=160 µm) at a velocity $\boldsymbol{u_l}=u_l\boldsymbol{e_x}$, where $\boldsymbol{e_x}$ is the unit vector along the x axis. The polymer solution is exposed to thermal stimuli with two different time intervals of either Δt_f=2($L - x$)/u_l in the forward direction or $\Delta t_r = 2(L + x)/u_l$ in the backward direction; this corresponds to $\Delta V_{\tau,f}/V_0$=$\gamma(1 - e^{-\Delta t_f/\tau})\Delta T$ and $\Delta V_{\tau,r}/V_0$=$\gamma(1-e^{-\Delta t_r/\tau})\Delta T$ for a thermal viscoelastic coefficient respectively. By averaging the forward- and backward-moving microflows at x with $1/f_l$=($\Delta t_f + \Delta t_r$)/2, a novel form of microflow is

$$\boldsymbol{u}_{hf}(x) = -\boldsymbol{u_l}\sinh\left[\frac{2x}{u_l\tau}\right](\beta_0 + \beta_1 c_0^p S_T^p)(\gamma - \Gamma_\tau)(\Delta T)^2, \quad (2)$$

where $u_l = 2f_l L$. The hyperbolic sine function in Eq. (2) immediately leads to $u_{hf}(x) \propto -x$ for a small x. The microflows originating from the two ends propagate against one another and collide at the midpoint (FIG. 3(b)), leading to light-driven hydrodynamic focusing (LHF).

To experimentally test Eq.(2), we created a moving hot spot that moves in a 5.0$wt\%$ PEG solution by sweeping the laser spot back-and-forth along the line with 2L=160 µm. We measured the spatial profile of local microflow through particle image velocimetry with tracer particles of 3.0 µm silica beads. As shown in FIG. 3(c), $u_{hf}(x)$ at various velocities u_l clearly exhibits a flow oriented toward the midpoint from both edges. The change of the flow velocity as function of the distance from the midpoint is consistent with the analytical prediction. Remarkably, $\gamma - \Gamma_\tau$ in Eq.(2) means that this microflow disappears if the viscoelastic relaxation τ falls to zero, e.g., in glass substrates. Viscoelastic expansion is the key to drive LHF by sweeping a heat source.

G. Thermal molecular focusing

Key finding of LHF motivated us to investigate whether the interplay among phoretic transports (thermophoresis and diffusiophoresis) and LHF underlies tun-
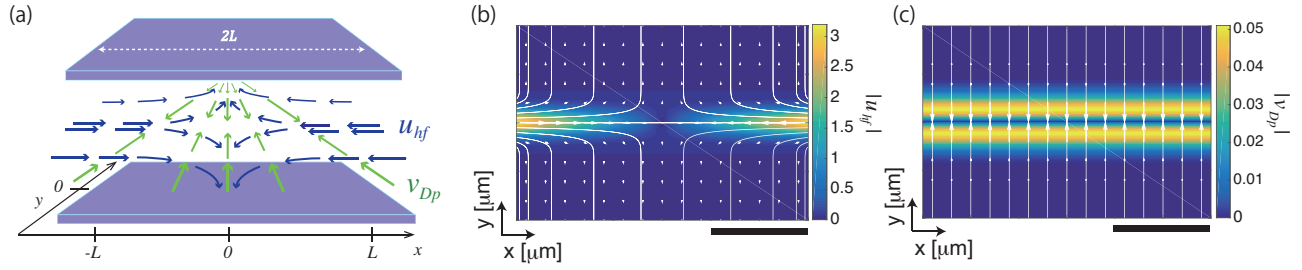
FIG. 4. The interplay between LHF and phoretic transports. (a) Schematic illustration of interplay between light-induced hydrodynamic focusing and diffusiophoresis. (b) A color-map of flow speed in the x direction, $|u_{hf}|$ obtained from numerical calculation, is simultaneously shown with its streamline (white) in a two-dimensional plane. (c) A color-map of the diffusiophoretic flow in the y-direction, $|v_{Dp}|$ obtained from numerical calculation, is also shown with its streamline (white). Scale bars: $100\,\mu$m.

able molecular focusing of DNA. We define the density flux of DNA by $\boldsymbol{J} = \boldsymbol{J}_{diff} + \boldsymbol{J}_{Tp} + \boldsymbol{J}_{Dp} + \boldsymbol{J}_{hf}$, where normal diffusion (first term), thermophoresis (second), diffusiophoresis (third), and LHF (fourth) are considered, and the net flux $\boldsymbol{J}$ is

$$\boldsymbol{J} = -D(\boldsymbol{\nabla}c + cS_T\boldsymbol{\nabla}T) + c\boldsymbol{u}_{Dp} + c\boldsymbol{u}_{hf}, \qquad (3)$$

where c is the concentration of DNA, D and S_T the diffusion coefficient and the Soret coefficient of DNA respectively (S_T=0.38 K^{-1}). Because diffusiophoresis of DNA in $5.0wt\%$ PEG solution becomes dominant rather than thermophoresis[23][24], the interplay of LHF $\boldsymbol{u}_{hf}$ and diffusiophoresis $\boldsymbol{u}_{Dp}$ decides where DNA is accumulated (FIG. 4(a)). $\boldsymbol{u}_{hf} = (u_{hf}, v_{hf})$ conveys DNA to a stagnation point at the center whereas diffusiophoresis $\boldsymbol{u}_{Dp} = (u_{Dp}, v_{Dp})$ captures DNA along x axis. Accordingly, the DNA is focused at the mid-point.

We next solve Eq. (3) at the steady state ($\boldsymbol{J}$=0, the DNA concentration at infinity is c_0) to analyze the focusing of DNA in detail. If the recovery of depleted PEG along the x axis, which is $w^2/D^p \approx$15 sec, takes longer than the period of a moving hot spot $1/f_l$, the gradient of PEG can be assumed to be stable. As for $f_l \geq 0.1$ Hz, we consider $\partial_x c^p$=0 and $\partial_y c^p$ no longer depends on time, i.e. $c^p(x,y) \approx c^p(y) = c_0^p \exp[-S_T^p \Delta T(y)]$. Diffusiophoresis transports DNA perpendicular to the laser path with $u_{Dp} = 0$ and $v_{Dp} = \frac{k_B T}{3\eta}\lambda^2(S_T^p - \frac{1}{T})c^p(y)\partial_y T$[23][24] (FIGs. 4(b) and (c)). Moreover, because v_{Dp} in $5.0wt\%$ PEG with $\nabla T \approx 0.1$ K/μm is much larger than v_{hf}, Eq. (3) is deduced to

$$J_x = -D(\nabla_x c + cS_T\nabla_x T) + cu_{hf}, \qquad (4)$$
$$J_y = -D(\nabla_y c + cS_T\nabla_y T) + cv_{Dp}. \qquad (5)$$

By solving Eqs. (4) and (5) at the steady state, the concentration of focused DNA is

$$c(x,y) = c_0 \exp\left[-S_T\Delta T + V'\Delta c^p + \frac{1}{D}\int_{-\infty}^{x} u_{hf}(x')dx'\right], \qquad (6)$$

where $\Delta c^p = c_0^p - c^p$ is the depleted amount of PEG and $V' = 2\pi a\lambda^2$ the effective volume involved

in diffusiophoresis with a depletion layer of thickness of λ (λ is comparable to $R_g^p \approx$2.5 nm). FIG. 5 shows the normalized concentration of focused DNA of $c(0,0)/c_0$. This analytical result agrees well with the experiment entirely for f_l=0.02 to 200 Hz. Moreover, this model describes the strategy to reinforce the LHF. The amplification rate of molecular focusing is defined as $A(x) = \exp[1/D\int_{-\infty}^{x} u_{hf}(x')dx']$ and $\ln A(0) \approx \frac{u_l^2\tau}{2D}\beta(\gamma - \Gamma_\tau)(\Delta T)^2$ means that molecular focusing is enhanced at the elastic substrate with large viscoelastic constant τ.

An intriguing observation is the frequency dependence. FIG. 5 shows that the curve of trapped DNA amount has a peak at an intermediate frequency of f_l=3.2 Hz, and then decreases at $f_l \geq 1/\tau$. A hot spot moving at higher frequency was also unable to enhance DNA accumulation. It is because PDMS is a thermal insulation material with low coefficient of heat transfer and enables varying ΔT in a frequency dependent manner. Heat conduction across the wall is evaluated based on thermal diffusion
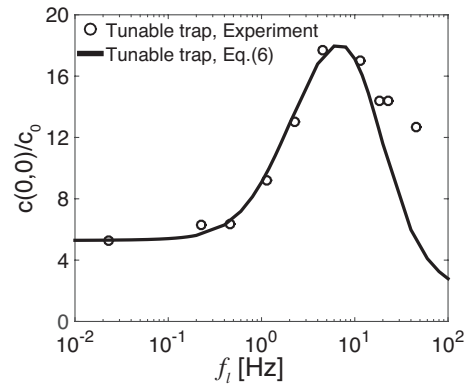

FIG. 5. Frequency-tunable molecular focusing of DNA. The black circle represents normalized amount of DNA in experiment, $c(0,0)/c_0$, and the black line is the numerical calculation of Eq. (6). Temperature difference ΔT was calculated from Eq.(7) using the following parameters[28][32][33]: C_v=4.2 × 10^{-12} J μm^{-3} K^{-1}, λ_h=6.1 × 10^{-7} W μm^{-1} K^{-1}, and h=5.0 × 10^{-10} W μm^{-3} K^{-1}.

equation in a two-dimensional space[28]:

$$C_v \frac{\partial(\Delta T)}{\partial t} - \lambda_h \nabla^2(\Delta T) = P - h\Delta T, \qquad (7)$$

where C_v and λ_h are the heat capacity and the heat diffusion coefficient of water respectively, $P = P_0 \exp[-((x - u_l t)^2 + y^2)/(2b^2)]$ with radius of $b=7.5\,\mu m$ is thermal energy from the laser spot, and h is the thermal transfer coefficient that represents heat sink toward PDMS from the solution[32][33]. ΔT also has a frequency dependence as ΔT starts to be reduced at a higher frequency $f_l \geq 2\pi h/C_v \approx 19\,Hz$. Thus, the temperature difference weakened at higher frequency results in the non-monotonic, resonance-like accumulation of DNA for sweeping frequency.

CONCLUSIONS

In this letter, we presented frequency-dependent microflow under a moving heat spot in a PEG solution that resulted from the coupling of viscoelastic expansion of fluids, and slow thermophoresis-induced viscosity reduction. Because diffusiophoretic trapping of DNA by the gradient of the PEG polymer overcomes its thermophoretic escape, the DNA advected by microflow is further focused through local hydrodynamic focusing. The speed of the microflow is controlled in a frequency-tunable way with no need of adjusting the experimental parameters, bringing technical advantages compared with the conventional methods. Further exploration in nematogenic microfluidics[32][33][34][35] and in a living cell[36] are promising applications. The conceptual advance obtained here is also relevant to seemingly disparate phenomena such as light-induced collective cell migration[37][38]. It would be of interest that such detailed investigation calls for new challenges to bridge the gap between physics and biology.

[1] G.I. Taylor, Proc. Royal Soc. London A, 1951, **209**, 447.
[2] M. Jaffrin and A. Shapiro, Annu. Rev. Fluid Mech., 1971, **3**, 13.
[3] H. Schmidt and A.R. Hawkins, Nat. Photon., 2011, **5**, 598.
[4] J.G. Cuennet, A.E. Vasdekis, L. De Sio, and D. Psaltis, Nat. Photon., 2011, **5**, 234.
[5] J.B. Knight, A. Vishwanath, J.P. Brody, and R.H. Austin, Phys. Rev. Lett., 1998, **80**, 3863.
[6] A. Shenoy, C.V. Rao, and C.M. Schroeder, Proc. Natl. Acad. Sci. U.S.A., 2016, **113**, 3976.
[7] G.M. Whitesides, Nature, 2006, **442**, 368-373.
[8] E. Yariv and H. Brenner, Phys. Fluids, 2004, **16**, L95.
[9] F.M. Weinert, J.A. Kraus, T. Franosch, and D. Braun, Phys. Rev. Lett., 2008, **100**, 164501; F.M. Weinert and D. Braun, Nano Lett., 2009, **9**, 4264.
[10] D. Pal and S. Chakraborty, Phys. Rev. E, 2012, **86**, 016321.
[11] N. Osterman and D. Braun, Appl. Phys. Lett., 2015 **106**, 073508.
[12] J.N. Pedersen, C.J. Luscher, R. Marie, L.H. Thamdrup, A. Kristensen, and H. Flyvbjerg, Phys. Rev. Lett., 2014, **113**, 268301.
[13] A. Würger, Phys. Rev. Lett., 2016, **116**, 138302.
[14] M. Braun and F. Cichos, ACS Nano **7**, 11200-11208 (2013); M. Braun, A. Würger, and F. Cichos, Phys. Chem. Chem. Phys., 2014, **16**, 15207.
[15] L. Lin, X. Peng, X. Wei, Z. Mao, C. Xie, Y. Zheng, ACS Nano, 2017, **11**, 3147.
[16] J.L. Anderson, Ann. Rev. Fluid Mech., 1989, **21**, 61.
[17] B. Abécassis, C. Cottin-Bizonne, C. Ybert, A. Ajdari, and L. Bocquet, Nature Materials, 2008, **7**, 785.
[18] J. Palacci, B. Abécassis, C. Cottin-Bizonne, C. Ybert, and L. Bocquet, Phys. Rev. Lett., 2010, **104**, 138302.
[19] B. Selva, L. Daubersies, and J.-B. Salmon, Phys. Rev. Lett. **108**, 198303 (2012).
[20] D. Florea, S. Musa, J.M.R. Huyghe, and H.M. Wyss, Proc. Natl. Acad. Sci. U.S.A., 2014, **111**, 6554.
[21] S. Shin, E. Um, B. Sabass, J.T. Ault, M. Rahimi, P.S. Warren, and H.A. Stone, Proc. Natl. Acad. Sci. U.S.A., 2015, **104**, 20167.
[22] N. Shi, R. Nery-Azevedo, A.I. Abdel-Fattah, and T.M. Squires, Phys. Rev. Lett., 2016, **117**, 258001.
[23] H.R. Jiang, H. Wada, N. Yoshinaga, and M. Sano, Phys. Rev. Lett., 2009, **102**, 208301.
[24] Y.T. Maeda, A. Buguin, and A. Libchaber, Phys. Rev. Lett., 2011, **107**, 038301.
[25] Y.T. Maeda, T. Tlusty, and A. Libchaber, Proc. Natl. Acad. Sci. U.S.A., 2012, **109**, 17972.
[26] Y.T. Maeda, Appl. Phys. Lett., 2013, **103**, 243704.
[27] T. Fukuyama, A. Fuke, M. Mochizuki, K. Kamei and Y.T. Maeda, Langmuir, 2015, **31**, 12567.
[28] Detailed description about theoretical model are presented in Supplementary information.
[29] J. Chan, J.J. Popov, S. Kolisnek-Kehl, and D.G. Leaist, J. Solut. Chem., 2003, **32**, 197.
[30] R. Holyst, et al., Phys. Chem. Chem. Phys., 2009, **11**, 9025.
[31] D. Niu, et al., Sci. Rep., 2016, **6**, 27366.
[32] D. Erickson, D. Sinton, and D. Li, Lab on a Chip, 2003, **3**, 141.

[33] H.M.J.M. Wedershoven, C.W.J. Berendsen, J.C.H. Zeegers, and A.A. Darhuber, Phys. Rev. Applied, 2015, **3**, 024005.

[34] Y-K. Kim, B. Senyuk, and O.D. Lavrentovich, Nat. Commun., 2012, **3**, 1133.

[35] M. Škarabot, N. Osterman, and I. Muševič, Soft Matt., 2017, **13**, 2448.

[36] M. Mittasch, et al. Nat. Cell Biol., 2018, **20**, 344.

[37] K. Aoki, et al. Dev. Cell, 2017, **43**, 305.

[38] S. Yabunaka and P. Marcq. Soft Matt., 2017, **13**, 7046.